

COVER PAGE

Document downloaded by @DAEL

Sat Nov 7 08:45:15 2026
For personal use

When automatic English translation is provided, only the original document is authentic.
The EAA cannot be held responsible of any translation error

Bibliographical reference

A Model to Predict Sound Reflections from Cliffs, Reto Pieren and Jean-Marc Wunderli, Acta Acustica **vol. 97** (Number 2), 2011, pp. 243-253

DOI
https://doi.org/10.3813/AAA.918404

ACTA ACUSTICA UNITED WITH ACUSTICA
Vol. 97 (2011) 243 – 253

DOI 10.3813/AAA.918404

A Model to Predict Sound Reflections from Cliffs

Reto Pieren, Jean Marc Wunderli
Empa, Swiss Federal Laboratories for Materials Science and Technology, 8600 Duebendorf, Switzerland.
[reto.pieren,jean-marc.wunderli]@empa.ch

Summary
In the context of the Swiss railway noise calculation model *sonRAIL* a model to predict sound exposure level spectra for reflections from cliffs was developed and validated with measurements. It is an engineering model with low computational cost that is applicable to any type of sound sources. The scattered energy reflected from the cliffs is modelled by the superposition of secondary sources placed on the cliff surface. The only free parameter of the model, the scattering coefficient, was determined by measurements with detonations of 200 g TNT_{eq} in the alpine part of Switzerland. Measurements yielded good agreement not only in situations with reflecting cliffs but also in the presence of large boulder fields.

PACS no. 43.50.+y, 43.28.En, 43.28.Js

1. Introduction

Reflections from cliffs can have a significant influence on sound exposure, mainly in cases where either the sound source or the receiver is close to a large cliff formation. In situations where the direct sound is shielded, the reflection from the cliff can even become the dominant sound path. In narrow valleys as often occur in the Alps these reflections produce long lasting echoes that are audible even at greater distances from the sound sources. Especially in the case of traffic noise, the inhabitants of such valleys often demand that these reflections be properly taken into account in sound propagation calculations. Hence it was decided for the new Swiss railway noise model *sonRAIL* [1] to develop a separate model for cliff reflections. The model should be formulated independently of a specific source type and, as it had to be implemented in an engineering model, great attention should also be drawn to keep the calculation demand small.

In sound propagation modelling there are several reflection phenomena apart from cliffs to deal with such as ground reflections or reflections by artificial objects like building facades or noise barriers. State of the art for the calculation of ground reflections are solutions for the reflection of spherical waves such as introduced by Chessel [2]. In *sonRAIL* this approach is used in combination with a frequency-dependent ground impedance model according to Delany and Bazley [3]. The solution is additionally extended to uneven terrain and varying ground properties by using a Fresnel zone concept. Reflections by artificial objects are often dealt with by applying a mirror source approach [4] or as recently proposed by solving Kirchhoff-Helmholtz integrals [5]. In the case of reflections from natural objects there exist prediction models for reflections by forest edges. Recently, a method where the reflection from a single tree was modelled by the scattered energy from a cylinder was presented [6]. However to the best of our knowledge no model for reflections from cliffs has been published so far.

Already a rough estimate of the resulting calculation times shows that the aforementioned approaches to deal with reflections by artificial objects are far too laborious against the background of the widespread reflecting areas that have to be taken into account for cliffs. Therefore it was decided instead to follow a common concept of room acoustics which represents reflections as the superposition of a specularly and a diffusely reflected part [7] [8]. The latter corresponds to the sound energy that is diffracted or scattered at a reflecting surface. The energy of the two contributions are related by the scattering coefficient which is dependent on the structure and size of the reflector as well as frequency and the angle of reflection. An excellent overview of measurement techniques and prediction methods for the scattering coefficient can be found in the book or article by Cox et al [9] [10].

The basis data of the presented model is a digital terrain model (DTM) which contains the height of every (x, y) coordinate pair. Therefore overhangs can not be represented by the DTM and the calculation model is limited to non-overhanging structures. With this assumption for typical valley situations where the source and the receiver points are located at the valley bottom, specular reflections are oriented towards the sky. Hence, in this context specular reflections can be neglected and only diffuse reflections from cliffs have to be taken into account. This corresponds to a major simplification as the superposition of different reflected contributions only has to be performed energetically. Thus, the presented model is limited to cases without

Received 14 July 2010,
accepted 15 December 2010.

© S. Hirzel Verlag · EAA

Document downloaded by @DAEL, 2026-11-07 08:45:17 - personal use only

overhangs or other geometries providing specular reflections.

The model that was derived on the basis of this assumption is presented in detail in the following section. In sections 3 to 5 the model is calibrated and compared with measurements. Section 6 shows a set validation measurements in a more complex situation with not only cliffs but large fields of boulders. The results are finally discussed in section 7.

2. Model

2.1. Introduction of secondary sources

As a starting point cliff formations are given as polygons in a two dimensional horizontal coordinate system. Typically the size of a cliff formation (i.e. one cliff polygon) taken from the latest digital surface model (DSM) of Switzerland is much larger than 1000 m^2. These polygons are then segmented with a constant cell width and secondary sources are placed in the centre of each grid point as illustrated in Figure 1. The inclination of each segment is derived from an underlying topographical model.

In the first step of calculation each secondary source is supplied with energy from the primary source. The acoustic behaviour of the cliff surface is modelled by a scattering coefficient and a radiation directivity. In the second step of the propagation calculation from the secondary sources to the receiver location the contributions from all secondary sources are energetically summed up.

For the acoustic behaviour of the cliff surface a simple model with only few parameters is required, in order to avoid overfitting measurement data in the parameter tuning process. Therefore the scattering coefficient is chosen independently from the angle of incidence, i.e. a random scattering coefficient is used. The directivity of the secondary sources is modelled according to Lambert's law.

2.2. Calculation of the sound power level of a secondary source

Following ISO 9613-2 [11] the sound power level of the secondary sources are calculated according to equation (1).

$$L_{WS,i,j} = L_{W,i} - A_{\mathrm{div},i,j} - A_{\mathrm{atm},i,j} - A_{\mathrm{gr}} + C_{\mathrm{proj},i,j}. \qquad (1)$$

$L_{WS,i,j}$ is the sound power level of the secondary source j supplied by the primary source i where $L_{W,i}$ is the emitted sound power level of the primary source i. Attenuation terms for geometrical divergence of the sound field A_{div}, atmospheric absorption A_{atm} and ground effect A_{gr} are taken into account. An additional term C_{proj} represents the integration over the projected reflector surface to obtain the sound power level of the secondary source j.

Geometrical divergence is calculated with $A_{\mathrm{div},i,j} = 10 \cdot \log(4\pi r^2)$ and the atmospheric absorption is defined as $A_{\mathrm{atm},i,j} = \alpha_{\mathrm{atm}} r/1000$, with r being the distance between the primary source and the reflector centre and α_{atm} being

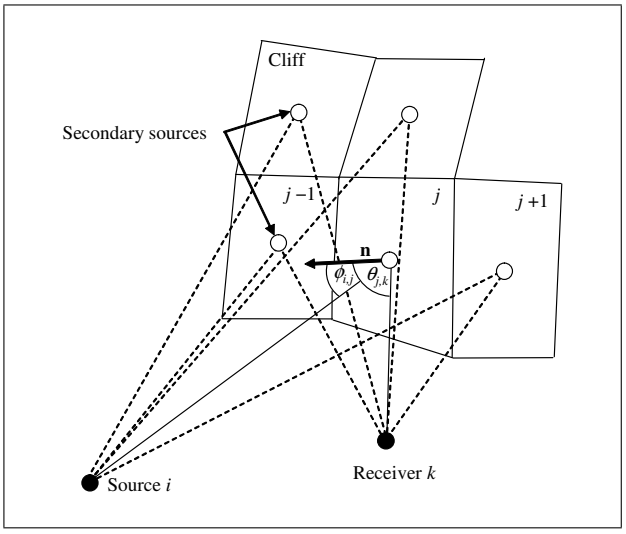


Figure 1. Illustration of the geometrical model for the calculation of reflections from cliffs by secondary sources (white circles).

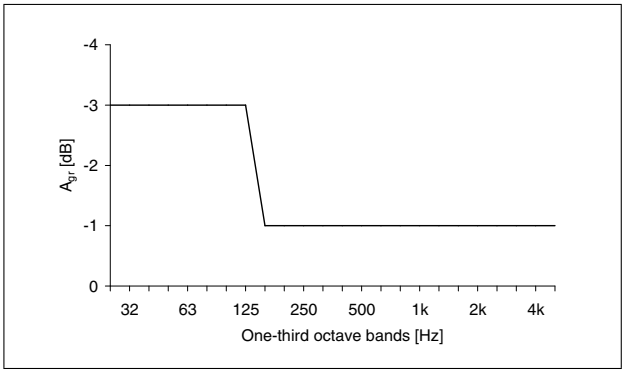


Figure 2. Simplified ground attenuation A_{gr} for the path from the primary source to the reflector and from the secondary source to the receiver, respectively.

the atmospheric attenuation coefficient according to [12]. There exist various methods for calculating the ground and barrier effect with engineering models such as [11], [13] or [14]. However, it was decided not to use one of these models but to implement a significantly less laborious approach in order to save calculation time. Considering the typical geometrical situation where sources as well as receivers are close to the ground but the reflecting surfaces are at greater distances and high above ground; calculations yield ground effect spectra that are very similar for most geometries. When also taking into account that the superposition includes contributions from a great number of secondary sources it can be deduced that pronounced ground effect dips will hardly ever occur. Therefore it was concluded not to do individual ground effect calculations for each propagation path but to rely instead on an integral, representative ground effect spectrum according to Figure 2. Up to a frequency of 160 Hz A_{gr} is set to -3 dB assuming energetic superposition of direct and reflected sound for both propagation path calculations. Due to sound absorption of porous ground at higher frequencies A_{gr} is increased to -1 dB. The barrier effect

Document downloaded by @DAEL, 2026-11-07 08:45:17 - personal use only

is only covered by a visibility check. Contributions from propagation paths that do not exhibit direct line of sight are neglected.

The reflector projection term $C_{\mathrm{proj},i,j}$ is calculated by equation (2).

$$C_{\mathrm{proj},i,j} = 10 \cdot \log\left(\cos(\phi_{i,j}) \cdot F_j\right). \tag{2}$$

It is assumed that the incoming sound intensity is constant over the reflector surface. So the integration of the incoming sound on the reflector can be calculated by the surface area F_j of the reflector j in m^2 and the angle $\phi_{i,j}$ between the incident sound path and the normal vector of the reflector j. Figure 1 illustrates the nomenclature of the situation.

2.3. Calculation of the sound exposure level at a receiver position

The sound exposure level at the receiver position k from the secondary source j which is supplied only by the primary source i is calculated by

$$L_{i,j,k} = L_{WS,i,j} - A_{\mathrm{div},j,k} - A_{\mathrm{atm},j,k} - A_{\mathrm{gr}} - A_{\mathrm{cliff},j,k}. \tag{3}$$

The attenuation terms describing the propagation path from the reflector j to the receiver position k are calculated in a manner analogous to equation (1). The acoustical properties of the cliffs are expressed by the attenuation term $A_{\mathrm{cliff},j,k}$ which is given by

$$A_{\mathrm{cliff},j,k} = A_{\mathrm{mat}} - D(\theta_{j,k}) - D_I. \tag{4}$$

The directivity of the secondary sources is described by the angular directivity gain $D(\theta_{j,k})$ and by the directivity index D_I which are given in equations (7) and (9), respectively. The properties of the reflector are introduced by the attenuation term A_{mat} that is calculated on the basis of the absorption and the scattering coefficient according to

$$A_{\mathrm{mat}} = -10 \cdot \log\left(s(1-\alpha)\right) \tag{5}$$

The frequency dependent scattering coefficient s is the ratio of the diffuse reflected energy to the total reflected energy. The absorption coefficient α represents the ratio of absorbed energy to the total incident sound energy. Both, the scattering coefficient and the absorption coefficient are assumed to be angle independent. The absorption coefficient α of cliffs can be assumed to be 0.

The radiation pattern of the secondary sources is modelled according to Lambert's cosine law. The angular directivity ratio Γ is defined as the ratio of the sound pressure at a specific angle to the sound pressure in the main radiation direction, both at a reference distance to the source. The angular directivity ratio Γ of the Lambertian radiator is given by

$$\Gamma^2_{\mathrm{Lambert}} = \begin{cases} \cos(\theta_{j,k}) & \text{if } \theta_{j,k} < \pi/2, \\ 0 & \text{else.} \end{cases} \tag{6}$$

where $\theta_{j,k}$ is the angle between the radiation direction and the normal vector of the surface [7]. The angular directivity gain of the secondary source is then given by

$$D(\theta_{j,k}) = 10 \cdot \log\left(\Gamma^2_{\mathrm{Lambert}}\right). \tag{7}$$

The directivity factor γ of the secondary source can be calculated by inserting equation (6) into the definition of the directivity factor and integrating over the surface of the unit sphere S:

$$\gamma \equiv \frac{S}{\oint \Gamma^2 \,\mathrm{d}S} = \frac{4\pi}{\int_0^{2\pi}\int_0^{\pi/2} \cos(\theta)\sin(\theta)\,\mathrm{d}\theta\,\mathrm{d}\varphi} = 4. \tag{8}$$

From equation (8) follows for the directivity index of the Lambertian radiator

$$D_I \equiv 10 \cdot \log(\gamma) = 6\,\mathrm{dB}. \tag{9}$$

The total immission level $L_{i,k}$ at a receiver position k induced by the primary source i can then be calculated by the energetic summation over the contributions of all secondary sources j

$$L_{i,k} = 10 \cdot \log\left(\sum_j 10^{L_{i,j,k}/10}\right). \tag{10}$$

3. Measurements

In order to determine the only free parameter of the model - the scattering coefficient - and to validate the proposed model, a series of measurements were carried out. The measurements were performed at a Swiss army exercise site in the alpine region. As sound source standard Swiss army exercise hand grenades were used that contain approx. 200 g $\mathrm{TNT_{eq}}$. Explosions are especially appropriate for this kind of measurements as they on the one hand produce enough sound power to yield clearly measurable echoes and on the other hand as impulse sources they allow the direct measurement of reverberation.

3.1. Measurement description

The measurement site was located in Chur and consisted of a grassy terrain with a large exposed cliff. The horizontal and vertical extent of the cliff are about 1 km and 80 m, respectively. The slope of the cliff lies between 120 and 170%. Figure 3 shows a panoramic view of the cliff in Chur seen from source position S5. Figure 4 yields a terrain profile from this position to the cliff. Additionally Figure 5 shows a sketch of the situation. The measurement positions of two sources S5 and S6 and receivers R14–R19 which were identified by GPS receivers are shown as well as the cliff formation. The shortest propagation distances source–cliff–receiver ranged from 175 m to 470 m. The microphones were placed upon elongated terrain banks of around 4 m height (marked as ellipses) with a microphone height of 4 m above terrain.

The measurements in Chur were performed on 10 July 2009 between 10:00 and 12:00 with fully clouded sky and

Document downloaded by @DAEL, 2026-11-07 08:45:17 - personal use only



Figure 3. Panoramic view of the measurement site in Chur, Switzerland.

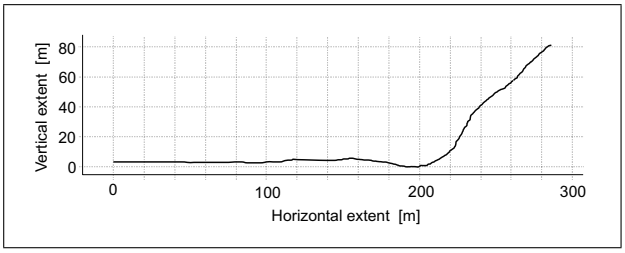


Figure 4. Vertical cut through the terrain from source position S5 perpendicular to the cliff. The source S5 is located at $x = 0$ m. At a distance of 200 m from the source the slope of the cliff starts.

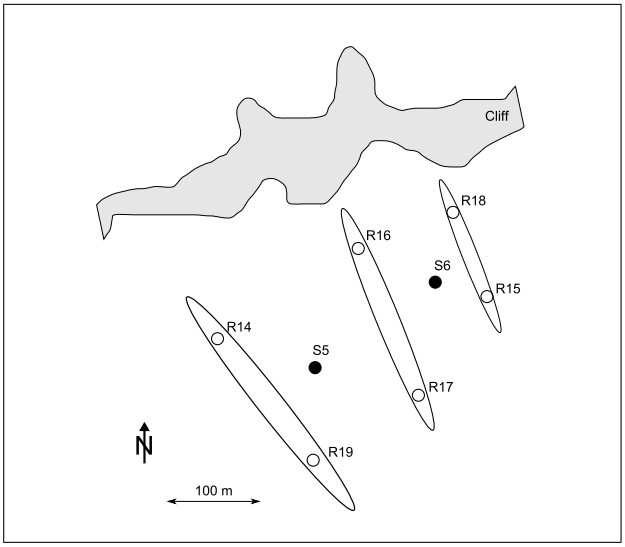


Figure 5. Sketch of the measurement situation in Chur, Switzerland. The situation shows 6 receiver positions R14 - R19 placed on elongated terrain banks (marked as ellipses) as well as two source positions S5 and S6 and the cliff.

light rain. The meteorological parameters temperature, humidity and wind were recorded. The wind vector was captured with an ultrasonic anemometer at height 10 m. The temperature increased during measurement time from 14.5 to 16.0 °C. The average wind direction was 74 ° corresponding to a wind from the east and the average wind speed was found to be 1.0 m/s. The relative humidity was approximately 85%.

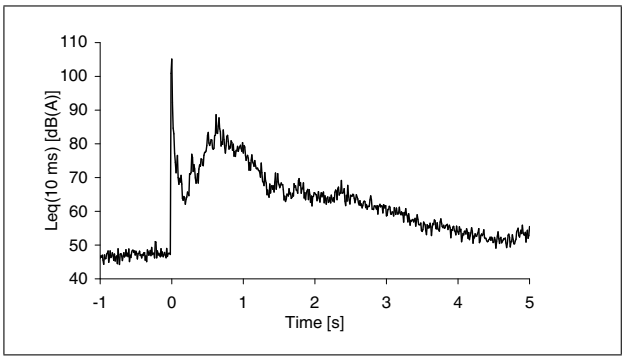


Figure 6. A-weighted level vs. time curve with 10 ms resolution for source position S6 and microphone position R14 in Chur.

At each source position 10 explosions were executed. The explosions were simultaneously recorded at six receiver positions with portable audio devices. As an example Figure 6 shows a level vs. time diagram for source position S5 and receiver position R14.

3.2. Postprocessing of measured data

For direct and reflected sound, sound exposure spectra were derived in one-third octave bands from 25 Hz to 5 kHz and energetically averaged over the measured single events. The sound exposure levels were corrected for background noise.

The separation of the direct sound (including ground reflections) and the reflections from the cliff was performed by temporal windowing of the recorded data. Rectangular windows with varying length depending on the geometrical situation were used. In some cases the difference of the propagation time of the first reflection from the cliff t_{cliff} and the propagation time of the direct sound t_{dir} was too small to ensure a sufficient temporal separation. Due to the temporal structure of the emission impulse this overlapping problem depends on frequency and is noticeable in low frequency bands only. Therefore frequency dependent quality criteria to account for the difference of the propagation times were introduced to ensure negligible influence of the direct sound on the calculated sound exposure level of the reflections from the cliffs. Only one-third octave band levels that met the criterion (11) were used for further analysis.

$$t_{\mathrm{cliff}} - t_{\mathrm{dir}} \geq T_{\mathrm{min},f}\,. \tag{11}$$

The values for $T_{\mathrm{min},f}$ were derived according to equation (12) on the basis of one-third octave band filtered sound pressure signals $p_f(t)$ of a pure direct sound impulse of total length T.

$$10 \cdot \log\left(\int_{T_{\mathrm{min},f}}^{T} p_f^2(t)\,\mathrm{d}t\right) = 10 \cdot \log\left(\int_0^T p_f^2(t)\,\mathrm{d}t\right) - B. \tag{12}$$

In the measured situations the sound exposure level of the cliff reflections usually lay around 20 dB below direct sound. In order to have a signal-to-noise-ratio of 10 dB the

Document downloaded by @DAEL, 2026-11-07 08:45:17 - personal use only

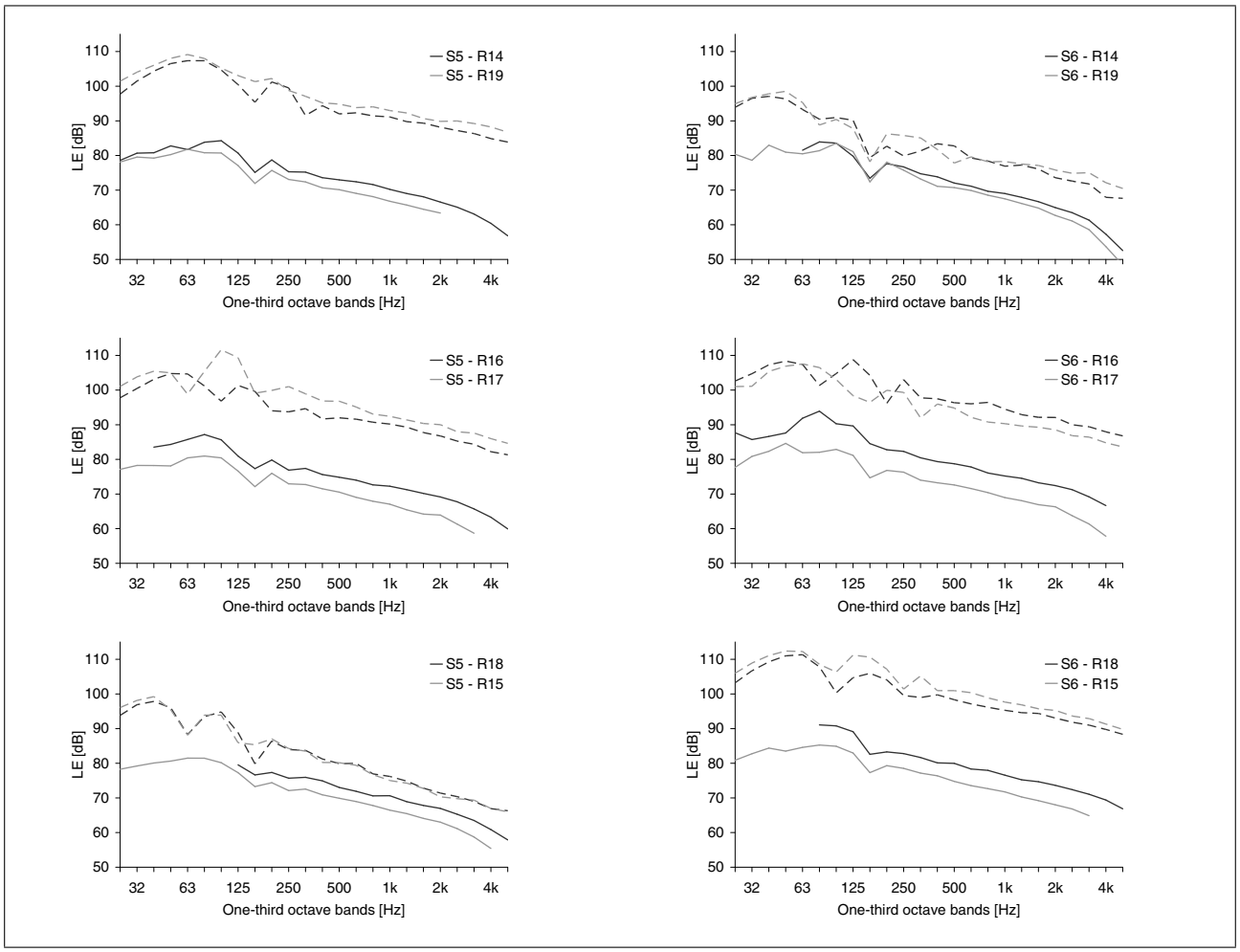


Figure 7. Measured sound exposure levels of reflections from cliffs (solid lines) and direct sound (broken lines) in one-third octave bands for different source and receiver positions.

threshold B was set to 30 dB. Criterion (11) only affected frequency bands below 125 Hz.

A second quality criterion concerning background noise was applied. Therefore in each one-third octave band the sound exposure level of the reflected sound $L_{E,\mathrm{refl},f}$ was compared with the corresponding background noise level $L_{eq,\mathrm{bn},f}$, calculated from a one-second window before each sound event. One-third octave bands that didn't meet the criterion (13) have been omitted:

$$L_{E,\mathrm{refl},f} > L_{eq,\mathrm{bn},f} + 10 \cdot \log T_{\mathrm{refl}} + C, \tag{13}$$

with T_{refl} being the integration time for the determination of $L_{E,\mathrm{refl},f}$ in seconds and C being a threshold. T_{refl} was 13 s and C was obtained by

$$C = -10 \cdot \log\left(10^{e/10} - 1\right). \tag{14}$$

The maximal error e was set to 0.5 dB. Criterion (13) only affected frequency bands over 2 kHz.

Measurement results are shown in Figure 7 where the sound exposure levels of direct sound and reflections are plotted. In all situations the sound exposure level of direct sound exceeds the sound exposure level of the reflections. The differences amount to around 10 to 20 dB. Below 250 Hz narrow banded dips and peaks are apparent which are assumed to stem from interferences due to ground reflections. Additionally Figure 8 contains the standard deviations of the measured sound exposure levels calculated from each series with 10 detonations. In most cases the standard deviations of the sound exposure levels of the reflected sound are below 1 dB. In contrast to this the standard deviation values of the direct sound typically exceed 1 dB and increase to higher frequency bands. Especially high standard deviation values for direct sound can be observed in situations S5-R15, S5-R18, S6-R14 and S6-R19 where a terrain bank is positioned between source and receiver point which can lead to shielding effects depending on the short-term weather conditions.

4. Determination of the scattering coefficient

From the measured data shown in section 3 the average scattering coefficient of the cliffs was determined. Each measured situation was reproduced by calculations according to the model presented in section 2 and the scatter-

Document downloaded by @DAEL, 2026-11-07 08:45:17 - personal use only

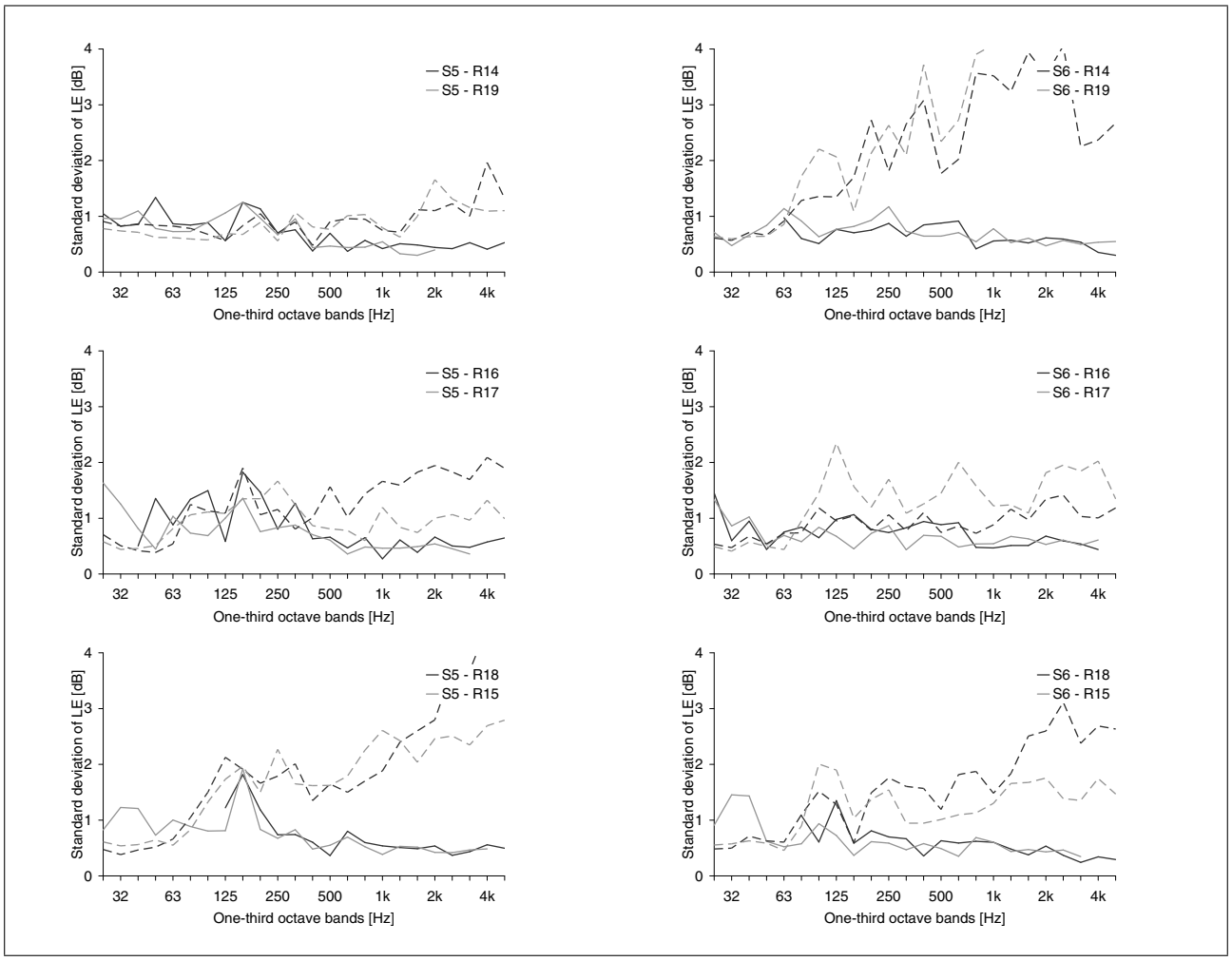


Figure 8. Standard deviations of measured sound exposure levels of reflections from cliffs (solid lines) and direct sound (broken lines) in one-third octave bands for different source and receiver positions ($N = 10$).

ing coefficient was adjusted to match the measured sound exposure levels.

4.1. Calculation setup

A digital terrain model (DTM) with 5 m resolution delivered the geometry of the cliffs and from a digital surface model (DSM) from the Swiss Federal Office of Topography *swisstopo* the cliff areas were extracted. The cliff areas were segmented into horizontal square cells of constant length. At the centre of each cell a secondary source with a specified height and orientation was placed. The orientation was determined by the mean normal vector of two planes defined by two triplets of edge points. To investigate the influence of the cliff resolution, calculations with different cell sizes between 5 m and 50 m were performed. Figure 20 shows the emission data that was used. According to [15] the effective source height for a point source of the Swiss army exercise hand grenade was set to 0.8 m above ground. The atmospheric absorption was calculated based on measured temperature and relative humidity.

4.2. Idealised scattering coefficient

Figure 9a and 9b show the calculated cliff scattering coefficients for the back-scattered part towards a downhill direction for the 12 situations for a segmentation of 20 m and 5 m. The squares indicate the mean values of the 12 situations with vertical lines yielding the 95% confidence intervals. From these values idealised scattering coefficient curves (bold lines) for different cliff segmentations were derived.

5. Application of the idealised scattering coefficient

In order to examine the accuracy of the Lambertian scattering model and the idealised scattering coefficient, calculated and measured sound exposure levels of the 12 situations described in section 3 were compared. Figure 10 shows the differences of measured and calculated sound exposure levels in one-third octave bands derived with a cliff cell size of 5 m and the corresponding idealised scattering coefficient. The bold line shows the mean value of the 12 curves. From 200 Hz to 4 kHz the mean absolute errors of the model are smaller than 1 dB. Hence the sound exposure levels of the cliff reflections could be reproduced with good accuracy in this frequency range. Below 200 Hz the mean errors exceed 1 dB. The deviations in

Document downloaded by @DAEL, 2026-11-07 08:45:17 - personal use only

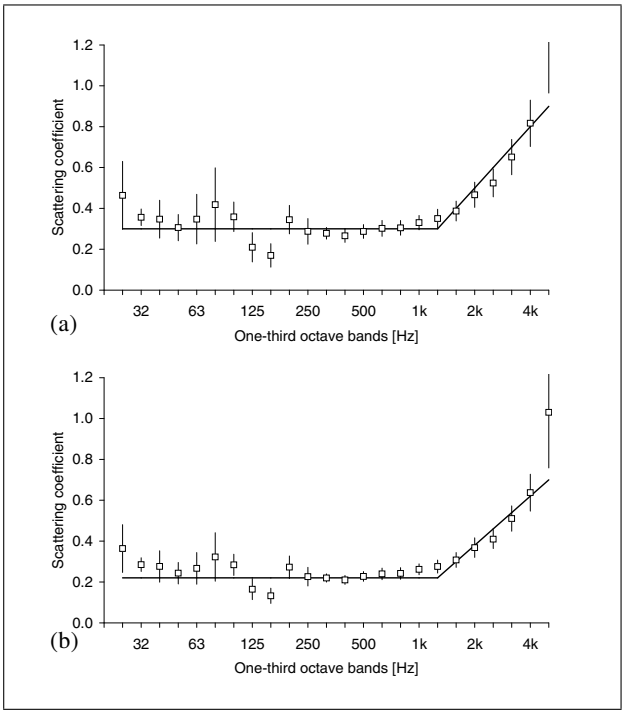


Figure 9. Cliff scattering coefficients for the back-scattered part towards a downhill direction determined by adjusting the proposed model to the measured situations for different cell sizes (squares with vertical lines indicating average values and 95% confidence intervals) and thereof derived idealised scattering coefficients (solid line) in one-third octave bands. a: Cliff cell size 20 m, b: Cliff cell size 5 m.

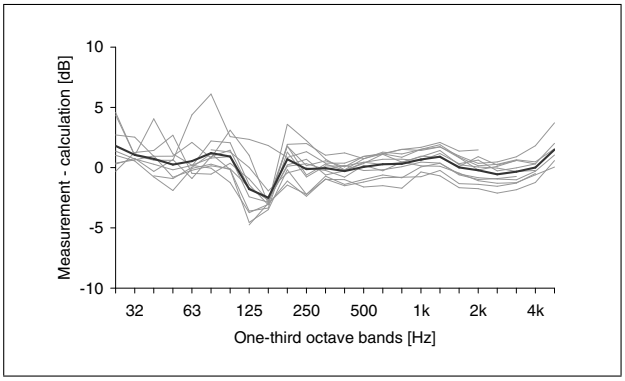


Figure 10. Differences of measurement and calculation of sound exposure levels of reflections from cliffs in one-third octave bands for 12 situations in Chur, Switzerland. The calculations were performed by the presented model with the idealised scattering coefficient from Figure 9b. The bold line shows the mean value of the 12 curves.

the lower frequencies most likely originate from the simplified ground effect model. However the inaccuracy of the model in the lower frequency bands has only a slight influence on the A-weighted values. Figure 11 shows the comparison of measured and calculated A-weighted sound exposure levels for the 12 situations. The errors of the A-weighted values exhibit a standard deviation of 0.9 dB(A). Compared to the range of absolute sound exposure levels,

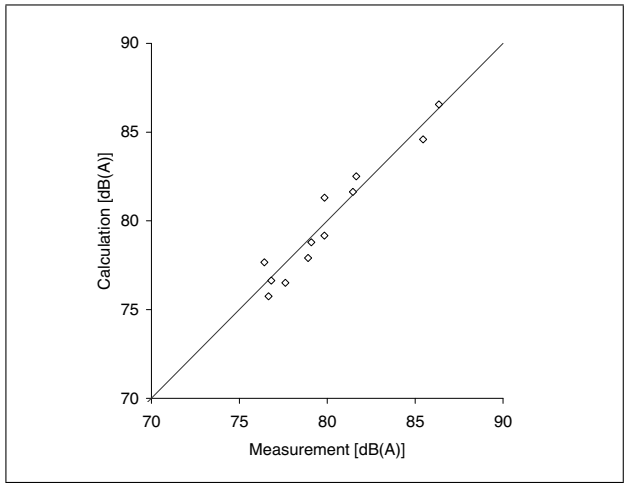


Figure 11. Calculation with the idealised scattering coefficient from Figure 9b vs. measurement of A-weighted sound exposure levels of sound reflections from cliffs for 12 situations in Chur, Switzerland.

which exceeds 10 dB(A), this suggests that the Lambertian scattering model is appropriate.

6. Validation

The depicted model was subsequently applied in a more common situation where not only cliffs but also boulders and trees were present. Although the model was developed for reflections from cliffs, identical settings were adopted for areas with boulders.

6.1. Measurements

Val Cristallina in Switzerland represents a characteristic alpine valley with steep inclinations and a relatively narrow valley floor. The inclinations consist of mixed cliff and boulder areas as well as small forests as illustrated in Figure 12. Figure 13 shows the valley floor which is partially covered with boulders. In Figure 14 a terrain profile of Val Cristallina is shown. Figure 15 shows a sketch of the measurement situation in Val Cristallina with the measurement positions. A total of 4 source positions S1–S4 and 13 receiver positions R1–R13 resulting in 18 measured propagation paths were used. Table I contains the Swiss National coordinates of the measurement positions. The propagation distances source–cliff–receiver ranged from 120 m to 620 m. The sound source consisted of 50 g charges of explosive material (Plastit), which were ignited on the ground.

One series of measurements in Val Cristallina was performed on 1 July 2009 between 16:30 and 17:10 with partly clouded sky and light rain. The mean temperature was 20.0 °C and the relative humidity 47%. The mean wind vector had a direction of 334 ° with magnitude 4.2 m/s. A second series of measurements was performed on 2 July 2009 between 9:00 and 10:40 in the morning with cloud-free sky. During the measurements the temperature rose from 13 to 17 °C and the relative humidityde-

Document downloaded by @DAEL, 2026-11-07 08:45:17 - personal use only



Figure 12. Cliff formation mixed with boulders and trees in Val Cristallina, Switzerland.



Figure 13. Photography of Val Cristallina, Switzerland, with large cliff formations in the background and boulders on the valley floor (seen from measurement position R3).

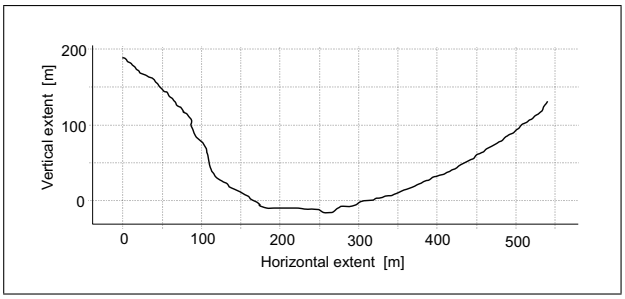


Figure 14. Vertical cut through the terrain of Val Cristallina perpendicular to the valley and through measurement position R13. Between $x = 50$ m and $x = 125$ m a large cliff formation with a slope of around 270% is present. Receiver position R13 was located at $x = 400$ m.

creased from 75% to 53%. The mean wind direction was 134 ° with an average wind speed of 0.6 m/s.

At each source position 8–10 explosions were executed. The explosions were simultaneously recorded at 4–5 receiver positions with portable audio devices. Figure 16

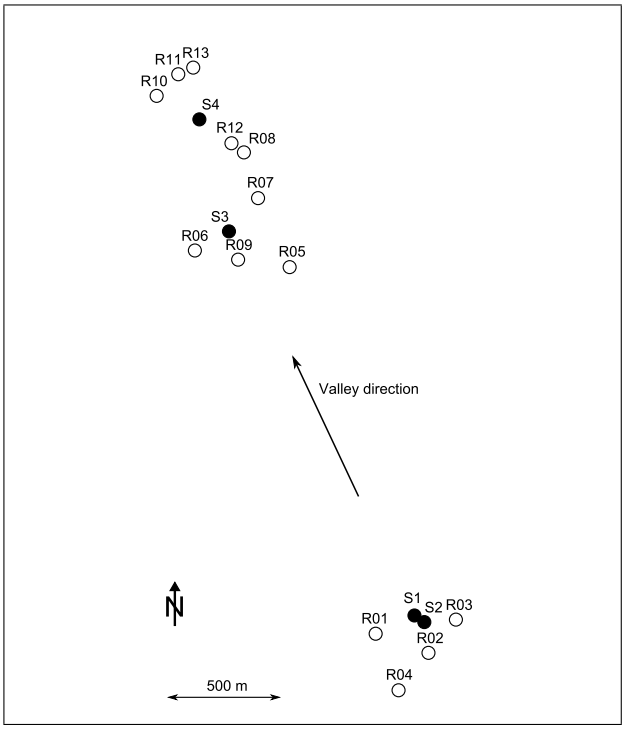


Figure 15. Sketch of the measurement situation in Val Cristallina, Switzerland. The situation shows 4 source positions (black circles) and 13 receiver positions (white circles). The valley direction is marked with an arrow.

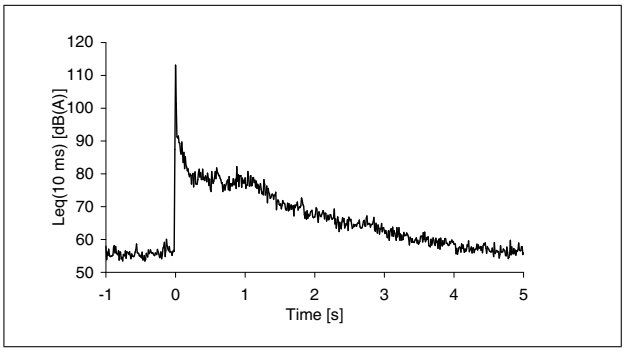


Figure 16. A-weighted level vs. time curve with 10 ms resolution for source position S4 and microphone position R13 in Val Cristallina.

shows an example of a measured level vs. time curve. Again for direct and reflected sound, sound exposure spectra were derived in one-third octave bands from 25 Hz to 5 kHz and averaged over the measured single events. The sound exposure levels were corrected for background noise.

For the temporal separation of direct sound (including ground reflections) and reflections from cliffs and boulders a fixed window length of 400 ms for the direct sound was used. The maximal error e of the background noise criteria (13) was set to 1.5 dB. Except for path S4-R09, which has a source receiver distance of 620 m, these criteria only affected frequency bands above 2.5 kHz.

Figure 17 shows the derived sound exposure spectra in one-third octave bands. Except for path S4-R09, where di-

Document downloaded by @DAEL, 2026-11-07 08:45:17 - personal use only

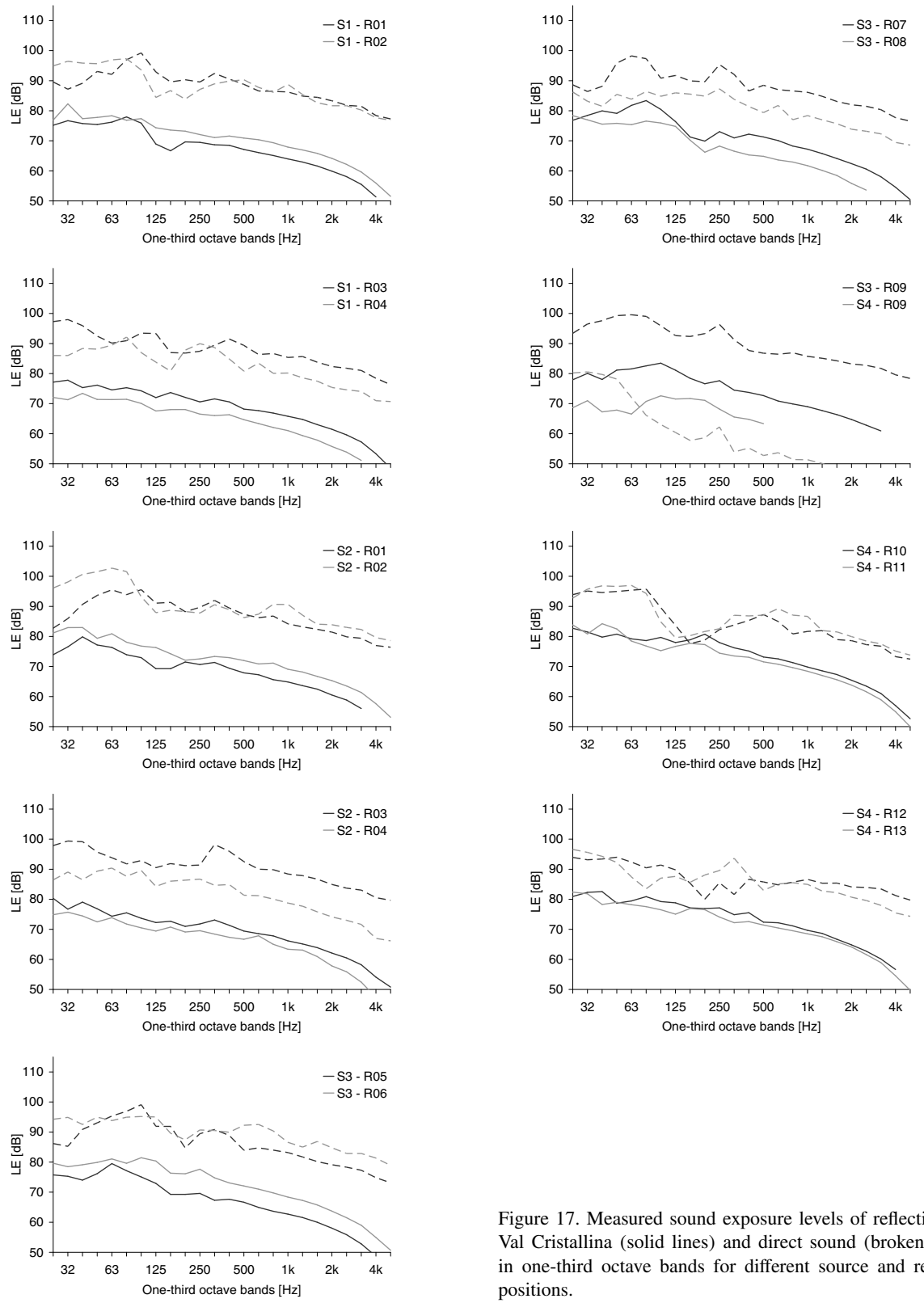


Figure 17. Measured sound exposure levels of reflections in Val Cristallina (solid lines) and direct sound (broken lines) in one-third octave bands for different source and receiver positions.

rect sound is shielded by a small natural wall, the sound exposure level of the direct sound (including ground reflections) exceeds the sound exposure level of the reflections from cliffs and boulders.

Document downloaded by @DAEL, 2026-11-07 08:45:17 - personal use only

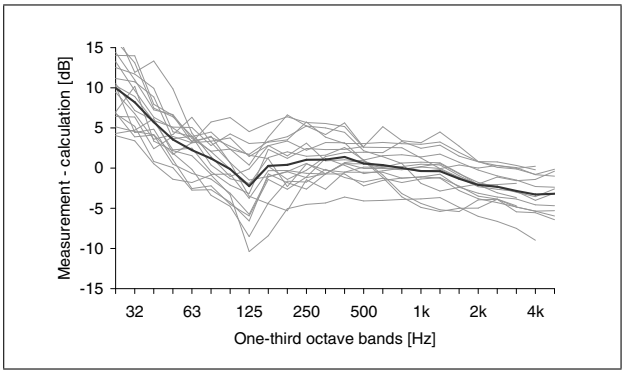


Figure 18. Differences of measurement and calculation of sound exposure levels of reflections from cliffs in one-third octave bands for 18 situations in Val Cristallina. The bold line shows the mean value of the 18 curves.

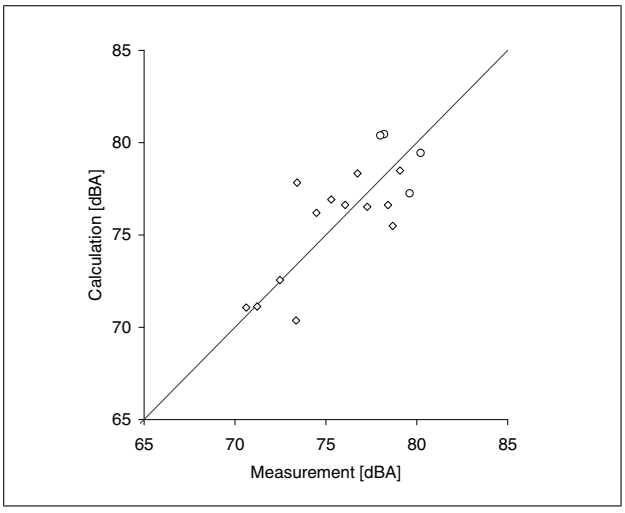


Figure 19. Calculation vs. measurement of A-weighted sound exposure levels of sound reflections from cliffs and boulders for 17 situations in Val Cristallina. Circles show situations, where a significant contribution of sound reflections from forest edges was calculated.

6.2. Calculation description

The sound propagation calculation was conducted as described in section 4.1 with a cliff cell size of 5 m. For boulder areas the same idealised scattering coefficient as for cliffs as shown in Figure 9b was used. Additionally a model for the calculation of reflections from forest edges (see [6]) was employed. The calculated levels of both models were energetically summed up. Figure 20 shows the emission data of the detonations. According to [15] the effective source height for a point source of the detonations was set to 0.7 m above ground.

6.3. Comparison of calculations and measurements

Figure 18 shows the differences between the measured and calculated sound exposure spectra for the 18 situations. Within the range 160 Hz to 1.25 kHz the mean error remains below 1 dB with standard deviations of around 2.7 dB. Above 1.25 kHz the calculations yield levels which are slightly too high compared to the measurements. Below 100 Hz the calculations systematically underestimate the measured values with a mean deviation of 3.6 dB at 50 Hz. It is remarkable that in spite of the mean error the standard deviation still stays relatively small with 2.8 dB at 50 Hz. The systematic errors in the lower frequencies seem to stem from the ground effect model which assumes energetic superposition of direct sound and a single ground reflection, i.e. -3 dB attenuation. On the one hand at low frequencies phase-dependent superposition should be considered involving -6 dB attenuation for a single reflection. On the other hand for valley situations with multiple ground reflections the focusing effect of the valley slope [16] can lead to ground effect attenuation terms even smaller than -6 dB. Therefore in order to reproduce the sound exposure levels in lower frequency bands a more elaborate ground effect model would be required.

The comparison of measured and calculated A-weighted values is shown in Figure 19. For propagation path S4-R09 due to the background noise no A-weighted value could be evaluated. Therefore only 17 propagation situations are shown. The mean deviation of the A-weighted sound exposure level is -0.3 ± 2.1 dB(A).

7. Discussion

It is peculiar to notice that the measured sound exposure level of reflections exhibit a smaller dispersion per series than direct sound levels (see Figure 8). This can be explained on the one hand by the fact that the sound propagation for the reflected part generally takes place high above ground and is therefore much less influenced by changes in meteorological conditions and ground properties. On the other hand a lot of reflectors contribute to the overall sound exposure resulting in an averaging over numerous propagation paths. This insensitivity to some of the major factors influencing sound propagation justifies the use of a simple propagation model that neglects meteorological influences and uses only a predefined ground effect spectrum.

One has to be aware though that such a simplified propagation calculation can lead to greater uncertainties when looking at single third-octave-bands. Even if ground effect is not very prominent there might be interference dips that are not reproduced by the calculations. Deviations between measurements and calculations may also be found in situations with relevant higher order reflections as these are not considered in the model. An additional restraint of application may be due to the geometry of source and receiver. As specular reflections are not taken into account in the model, situations with mirror source reflections can not be reproduced accurately.

In spite of these restraints the proposed model should be applicable in the vast majority of situations and is likely to yield accurate predictions of the resulting sound exposure level. The aforementioned limitations are not fundamental as the model could easily be extended to consider specular reflections and more sophisticated propagation algorithms. The additional computational requirements to extend the

Document downloaded by @DAEL, 2026-11-07 08:45:17 - personal use only

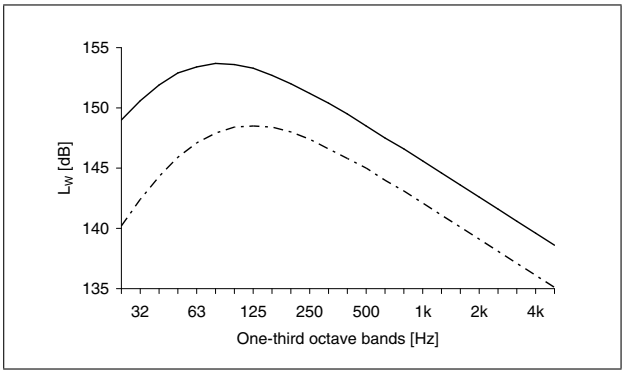


Figure 20. Source data used for modelling the measurement situations in Chur and Val Cristallina: Weber spectra (see [17]) of an explosion of a Swiss army exercise hand grenade (solid line) and of an explosion of 95g TNT_{eq} (broken line) on the ground in one-third octave bands according to [15]. Note: Non-linear effects of the source are integrated. The spectra are only valid for distances outside the non-linear region of the source.

range of application or increase the accuracy however is judged to be disproportional to the benefits and is therefore, at least for engineering models, not recommended.

8. Conclusion

The reflection model for cliffs yields a good accuracy in the prediction of A-weighted sound exposure level in a case with a mixture of cliffs and boulders. This is encouragement that the scattering coefficient derived just for cliffs is applicable for other kind of natural rocky surface. However, this assumption has to be confirmed by additional measurements.

It can be concluded that the presented model features a reasonable compromise between the wish for high accuracy and the demand for quick calculation algorithms as needed for engineering models.

Annex

Figure 20 shows the source data used for modelling the measurement situations in Chur and Val Cristallina. Table I contains the Swiss National coordinates of the measurement positions in Chur and Val Cristallina.

Acknowledgment

This work was supported by the Defence Procurement Agency of Switzerland (armasuisse) and the Federal Office for the Environment of Switzerland (bafu).

References

[1] D. Sehu, J. M. Wunderli, K. Heutschi, T. Thron, M. Hecht, A. Rohrbeck, T. Ledermann: sonRAIL - Projektdokumentation. Bundesamt für Umwelt (Bafu), 2010. http://www.bafu.admin.ch/laerm/01148/06762/07079/index.html?lang=de.

[2] C. I. Chessell: Propagation of noise along a finite impedance boundary. Journal of the Acoustical Society of America **62** (1977) 825–834.

[3] M. Delany, E. Bazley: Acoustical properties of fibrous absorbent materials. Applied Acoustics **3** (1970) 105–116.

Table I. Swiss National coordinates (SNC) of measurement positions in Chur and Val Cristallina.

Pos.	SNC	Pos.	SNC
S1	708605 / 161962	R8	707859 / 163968
S2	708634 / 161942	R9	707840 / 163508
S3	707797 / 163620	R10	707490 / 164210
S4	707669 / 164104	R11	707581 / 164304
S5	756652 / 191432	R12	707817 / 164001
S6	756791 / 191529	R13	707647 / 164331
R1	708429 / 161893	R14	756535 / 191466
R2	708661 / 161809	R15	756850 / 191516
R3	708779 / 161952	R16	756703 / 191572
R4	708528 / 161644	R17	756772 / 191400
R5	708063 / 163469	R18	756811 / 191613
R6	707655 / 163540	R19	756647 / 191326
R7	707924 / 163776		

[4] K. P. Lee, H. G. Davies: Nomogram for estimating noise propagation in urban areas. The Journal of the Acoustical Society of America **57** (1975) 1477–1480.

[5] K. Heutschi: Calculation of reflections in an urban environment. Acta Acustica United with Acustica **95** (2009) 644–652.

[6] J. M. Wunderli, E. M. Salomons: A model to predict the sound reflection from forests. Acta Acustica United with Acustica **95** (2009) 76–85.

[7] H. Kuttruff: Room acoustics. Applied Science Publishers Ltd, 1973. 0-85334-573-2.

[8] M. Vorlaender, E. Mommertz: Definition and measurement of random-incidence scattering coefficients. Applied Acoustics **60** (2000) 187–199.

[9] T. J. Cox, P. D'Antonio: Acoustic absorbers and diffusers - theory, design and application. Spon Press, 2004. 0-415-29649-8.

[10] T. J. Cox, B. I. L. Dalenback, P. D'Antonio, J. J. Embrechts, J. Y. Jeon, E. Mommertz, Vorl, M. nder: A tutorial on scattering and diffusion coefficients for room acoustic surfaces. Acta Acustica United with Acustica **92** (2006) 1–15.

[11] International Organization of Standardization: ISO 9613-2: Acoustics - Attenuation of sound during propagation outdoors, part 2: General method of calculation. 1996.

[12] International Organization of Standardization: ISO 9613-1: Acoustics - Attenuation of sound during propagation outdoors, part 1: Calculation of the absorption of sound by the atmosphere. 1993.

[13] D. van Maercke, J. Defrance: Development of an analytical model for outdoor sound propagation within the harmonoise project. Acta Acustica United with Acustica **93** (2007) 201–212.

[14] G. Dutilleux, J. Defrance, D. Ecotiere, B. Gauvreau, M. Berengier, F. Besnard, E. Le Duc: Nmpb-routes-2008: The revision of the french method for road traffic noise prediction. Acta Acustica United with Acustica **96** (2010) 452–462.

[15] J. M. Wunderli: Modelling the source strength of explosions under consideration of the ground influence. Acta Acustica United with Acustica **90** (2004) 690–701.

[16] K. Heutschi: On the sound propagation in alpine valleys. Euronoise 2006, Tampere, Finland, 2006.

[17] International Organization of Standardization: ISO/TS 13474: Acoustics - Impulse sound propagation for environmental noise assessment. 2003.

Document downloaded by @DAEL, 2026-11-07 08:45:17 - personal use only